Journal of Zhejiang University-SCIENCE A (Applied Physics & Engineering)
ISSN 1673-565X (Print); ISSN 1862-1775 (Online)
www.jzus.zju.edu.cn; www.springerlink.com
E-mail: jzus@zju.edu.cn

Effects of bleed hole size on supersonic boundary layer bleed mass flow rate*

Bao-hu ZHANG, Yu-xin ZHAO†‡, Jun LIU

College of Aerospace Science and Engineering, National University of Defense Technology, Changsha 410073, China

†E-mail: zhaoyuxin@nudt.edu.cn

Received Oct. 5, 2019; Revision accepted Jan. 4, 2020; Crosschecked July 16, 2020

Abstract: The bleed hole diameter, depth, and boundary layer thickness are key design parameters of a supersonic bleed system. The evolution trend of single-hole bleed flow coefficient with the ratio of boundary layer thickness to bleed hole diameter and the ratio of bleed hole depth to diameter is investigated by numerical simulations under choking and non-choking conditions. The results show that the subsonic leading edge of the circular hole and the subsonic part of the boundary layer are the main factors causing lateral flow of the bleed hole. The effect of diameter on bleed mass flow rate is due to the viscous effect which reduces the effective diameter. The larger the ratio of displacement thickness to bleed hole diameter, the more obvious the viscous effect is. The depth affects bleed flow rate by changing the opening and closing states of the separation zone. When a certain depth is reached, the development of the boundary layer reduces the effective captured stream tube and thus reduces the bleed mass flow rate. The main objective of the study is to obtain the physical mechanism of the bleed hole size parameters affecting the bleed mass flow rate, and to provide theoretical guidance for the selection of the size of bleed holes in the design of a porous arrays bleed system in hypersonic inlets.

Key words: Inlet; Supersonic bleed; Scale effects; Choking; Bleed mass flow rate; Lateral flow
https://doi.org/10.1631/jzus.A1900507 **CLC number:** V411

1 Introduction

Hypersonic aircraft rely on air captured by an inlet to meet the requirements of the propulsion system. The inlet serves also to condition the air through deceleration and pressurization, supplying air with specific temperature, speed, and pressure to the combustion chamber (Zhao, 2014). Its performance directly affects the performance of the propulsion system (Zhang et al., 2019). An important development design trend of the hypersonic inlet is not to seek the best performance of individual components, but to satisfy the performance index of the whole system of aircraft-engine-inlet, to ensure the high performance of the inlet under long-term cruise Mach number, and also to take into account the non-design point performance of the inlet under non-design Mach number (Hu et al., 2013), which requires effective flow regulation and control (Jiao, 2017; Wang, 2017). Boundary layer bleed is an effective method of inlet control (Soltani et al., 2015; Im and Do, 2018). The performance of the inlet can be significantly improved by setting an effective bleed hole layout in the inlet (Wang et al., 2015; Gupta et al., 2016; Zhang, 2018).

The bleed system is a porous array layout, which achieves the aim of flow control through effective bleed array layout (Hamed et al., 2011). The porous array bleed system has a certain porosity, which is used to control the overall bleed mass flow rate. The

‡ Corresponding author
* Project supported by the National Natural Science Foundation of China (No. 11472304) and the Graduate Innovation Grant of Hunan Province (No. CX2017B006), China
ORCID: Bao-hu ZHANG, https://orcid.org/0000-0002-2866-8761; Yu-xin ZHAO, https://orcid.org/0000-0001-8133-1829

determination of the bleed mass flow rate of the bleed system first needs to determine the single-hole bleed mass flow rate. Hypersonic inlet bleed includes forebody, throat, and lip bleed (Zhao, 2016). Each part has different requirements for the shape and size of bleed hole (Chang et al., 2017). If the bleed hole diameter is too large, the flow coefficient captured by the inlet will decrease, which reduces the efficiency of the combustion chamber. At the same time, the intensity of the barrier shock generated by the trail edge of the bleed hole will increase, and a large number of vortices will be induced, resulting in significant total pressure loss (Wukie et al., 2015). If the bleed hole diameter is too small, it will lead to insufficient bleed mass flow, which will not be effective in bleed control. On the other hand, the hypersonic inlet has a certain structural strength, so the bleed hole has a certain depth. In theory, there is an optimum scheme of bleed system design considering the boundary layer thickness, and the bleed hole diameter and depth, which makes the flow field distortion smallest and the control effect most effective when the bleed mass flow rate is as small as possible.

The performance of a hypersonic inlet bleed system depends on many factors, including the position, angle, and shape of the bleed hole. Martin et al. (2007) by computational fluid dynamics (CFD) showed that total pressure recovery increased by 2% by 1% bleed mass flow rate, 1% by 2% bleed mass flow rate, and almost the same by 4% bleed mass flow rate, indicating the existence of the best appropriate bleed mass flow rate. Syberg and Hickcox (1973) studied the influence of the inclination angle of the bleed hole, the distance between the holes, and the diameter of the hole on the bleed mass flow rate. The selected diameter of the bleed hole is equivalent to the displacement thickness of the boundary layer. Davis et al. (1997) by experiment showed that when the bleed hole diameter equals or is less than the boundary layer displacement thickness, the flow coefficient is approximately the same. Davis et al. (2012) experimentally obtained the variation trend of bleed flow coefficients with different back pressures at different depths and angles of the bleed hole, and compared it with existing data. Sepahi-Younsi et al. (2019) found that when the ratio of the depth to diameter of the bleed hole is large, the separation bubble at the front of the bleed hole is closed, but when the ratio of depth to diameter is small, the separation bubbles extend to the bleed chamber and the separation bubbles are in an open state. This easily causes flow instability.

In this paper, the single-hole problem is extracted from the porous array bleed layout, and the effect of the boundary layer thickness and the diameter and depth of the bleed hole on the bleed mass flow rate are studied to obtain single bleed hole performance. The main purpose is to obtain the physical picture of each parameter affecting the bleed mass flow rate, and to lay the foundation for extending the single-hole bleed system to the multi-hole bleed system, and then for the design of a simple and efficient advanced hypersonic inlet bleed system.

2 Numerical simulation methods and validations

Steady and density-based simulations are solved with the finite volume method. The inviscid terms are discretized by the second-order Roe scheme, and the viscous terms are discretized by the second-order central-difference scheme. The molecular viscosity of the gas is calculated with Sutherland's formulation. No-slip adiabatic wall conditions are applied for all solid surfaces and the turbulence is modeled by the k-ε two-equation model.

The integrated computer engineering and manufacturing (ICEM) is used to generate the structured grids, and the computational domain is halved because of symmetry as shown in Fig. 1. A C-type mesh is generated and refined in the bleed hole region. The minimum grid spacing is 1.0×10^{-3} mm in the turbulent boundary layers above the bleed surface to ensure a maximum y+ of 2.0 for the free stream Reynolds number investigated. The grid growth rate is 1.02, which ensures that there are enough cells within the boundary layer for the three different boundary layer velocity profiles investigated. A 2D mesh is created in the ICEM 3D computational domain by the association between the face with the bleed hole planes as shown in Fig. 2. The boundary condition is set to be interior to monitor the bleed mass flow rate, and the average values of the three planes are taken as the bleed mass flow rate. The convergence criterion for all CFD cases is that the variance of the bleed mass flow rate is within 1.0%.

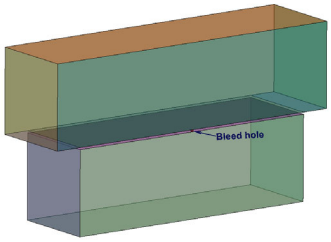

Fig. 1 Computational domain

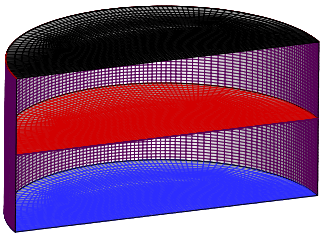

Fig. 2 Monitor planes of the bleed mass flow rate

Given the above grid topology, grid independent validation is carried out by selecting the bleed hole diameter D=2 mm, depth-to-diameter ratio L/D=0. The main purpose is to obtain the grid numbers and distributions in the mainstream, the bleed hole, and the bleed plenum regions. Five sets of grids are designed and the number of grids is 0.4271 million, 0.8576 million, 1.8245 million, 2.8726 million, and 3.5515 million (Fig. 3), respectively.

The flow coefficient (Willis et al., 1995) is defined as

$$Q=\frac{\dot{m}}{\dot{m}_{\text{sonic}}}, \tag{1}$$

where $\dot{m}$ is the actual bleed mass flow rate, and $\dot{m}_{\text{sonic}}$ is the sonic bleed mass flow rate, which is defined as

$$\dot{m}_{\text{sonic}}=\frac{P_{\text{t}}A}{\sqrt{T_{\text{t}}}}\sqrt{\frac{\gamma}{R}}\left(\frac{\gamma+1}{2}\right)^{\frac{\gamma+1}{2(1-\gamma)}}, \tag{2}$$

where P_{t} and T_{t} are the inflow total flow pressure and temperature respectively, γ is the specific-heat ratio, and A is the bleed hole area. R=287 J/(kg·K). The flow coefficients of five sets of grid with inflow pressure, temperature, Mach number, and back pressure are 101325.0 Pa, 288.15 K, 2.46, and 50662.5 Pa (Fig. 3).

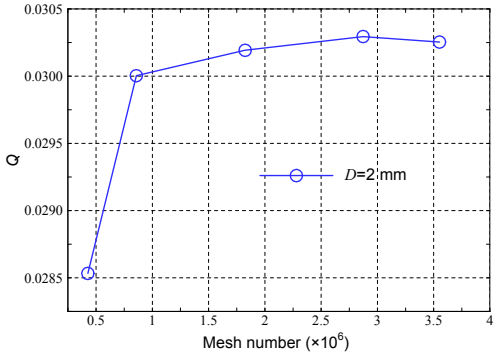

Fig. 3 Mesh independent validation

Fig. 3 shows that the fourth set of grids has met the requirements of grid independence. For the other computational examples with different diameters and depths, the mesh distribution is kept consistent in the regions of mainstream and bleed chamber, and only the mesh numbers in the bleed hole region are varied. With the increase of the ratio of the bleed hole depth to diameter, the number of meshes increases gradually, which requires a lot of high-performance computing resources.

To confirm the validation of the above numerical methods, the numerical results are compared with the experimental results conducted by Eichorn et al. (2013) with the Mach number Ma=1.7. A normal single-hole with a diameter D=6.350 mm and a depth-to-diameter ratio of 0.250 is selected, which is denoted as configuration No. 3 in the referenced paper. The Reynolds number for the test conditions is 2.46×10^7/m. The flow coefficient evolution with different ratios of bleed chamber static pressures P_{b} to incoming total pressure P_{t} is shown in Fig. 4.

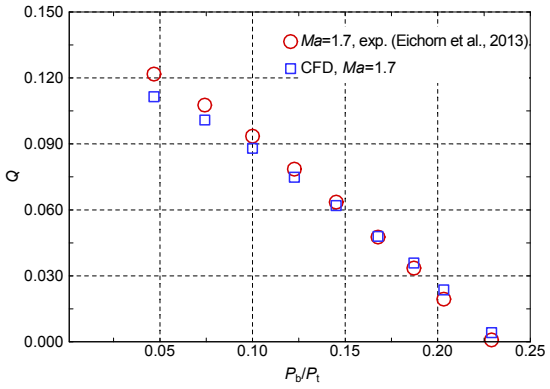

Fig. 4 Comparison of Eichorn et al. (2013)'s experiment and computational fluid dynamics

Fig. 4 shows that the numerical simulation results are in good agreement with the experimental results over a wide range of pressure ratios except for slight errors in low and high pressure ratios. Overall, this shows that the numerical simulation method is reliable and effective.

3 Evolution of flow coefficients with the ratio of boundary layer thickness to diameter

In order to enhance the efficiency of the compression process, the inlet designer must have a knowledge of the characteristics and vagaries of the boundary layer (Mahoney, 1990). The boundary layer has a velocity gradient, forming a three-layer structure (Babinsky and Harvey, 2011; Wang et al., 2017). The purpose of the boundary layer bleed is to change the shape factor of the boundary layer and make its profile much fuller (Bunnag, 2010). The hypersonic inlet bleed control system includes the forebody, lip, and throat bleed according to different demands. The leading edge of the bleed hole has different boundary layer thicknesses (δ) at different bleed positions. Given the relationship between the diameter of the bleed hole and the displacement thickness of the boundary layer, the boundary layer bleed can be divided into two cases. When the displacement thickness is much larger than the diameter of the bleed hole, this corresponds to subsonic bleed, and when the displacement thickness is smaller than the diameter of the bleed hole, the bleed is dominated by supersonic bleed. By changing the boundary layer thickness at the leading edge of the bleed hole, the influence of boundary layer thickness on the bleed mass flow rate is studied. The three velocity profiles at the leading edge of the bleed hole are shown in Fig. 5. The maximum boundary layer thickness is nearly nine times that of the minimum boundary layer thickness.

The curvature of the leading edge of a bleed hole varies continuously. For a certain inflow, it can be divided into supersonic leading edge and subsonic leading edge according to the relationship between the curvature of the leading edge and the Mach cone as shown in Fig. 6. The ratio of supersonic leading edge increases with the increases of Mach number. In order to eliminate the influence of subsonic and supersonic leading edges and the lateral flow caused by 3D effects, the influence of boundary layer thickness on bleed mass flow coefficient in 2D case is first studied.

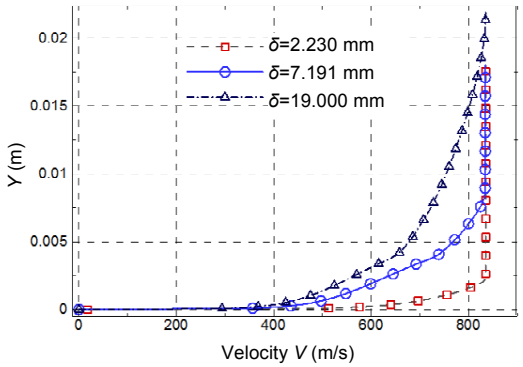

Fig. 5 Different velocity profiles at the leading edge of the bleed hole

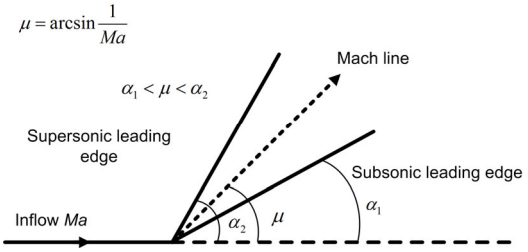

Fig. 6 Supersonic and subsonic leading edges for a circular hole

The 2D bleed slot diameter D equals 10 mm with the ratio of depth to diameter L/D=1.0. The incoming flow conditions are the same as the aforementioned mesh independent validation. For the case of δ/D=0.223, the Mach number contours with the ratios of the static pressure of the bleed chamber to inflow static pressure of 0.8 and 0.1 are shown in Fig. 7 and Fig. 8, respectively. By comparing Fig. 7 with Fig. 8, it can be seen that the supersonic streamlines deflect into the bleed hole by generating expansion waves at the leading edge of the slot through pressure difference. Different pressure ratios produce different expansion strengths. The lower the pressure ratio, the greater the streamline deflection angle, and the larger the bleed mass flow rate.

The bleed flow coefficients of the three boundary layer thickness-to-diameter ratios are shown in Fig. 9. It shows that with the decrease of pressure

ratio, the influence of boundary layer thickness on the flow coefficients becomes no longer obvious. The larger the ratio of boundary layer thickness to diameter, the smaller the flow coefficient is. This is because the thicker the boundary layer, the smaller the effective Mach number at the leading edge of the bleed slot, and the smaller the bleed mass flow coefficient.

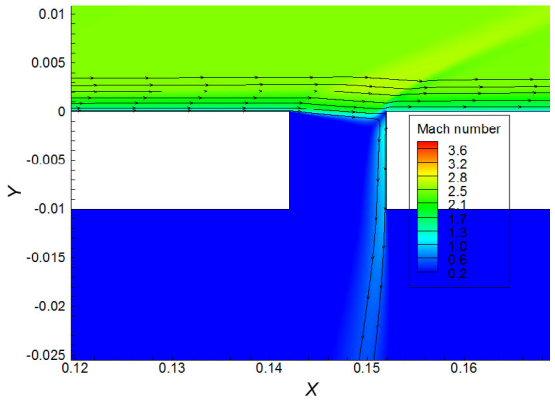

Fig. 7 Mach number contours for the slot with static pressure ratio of 0.8 and δ=2.230 mm

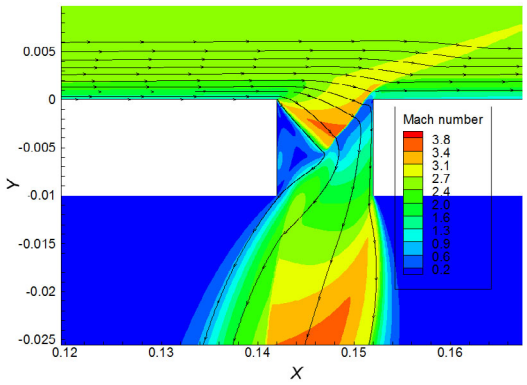

Fig. 8 Mach number contours for the slot with static pressure ratio of 0.1 and δ=2.230 mm

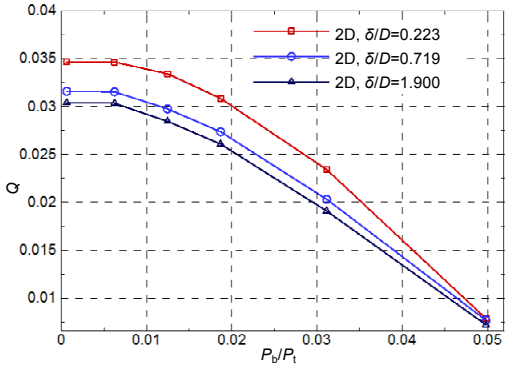

Fig. 9 Relationship between flow coefficient and P_b/P_t with different δ/D for the slot

The flow coefficient of the circular hole under the same inflow and boundary layer thickness as that in 2D cases of the slot is shown in Fig. 10. Comparison of Figs. 9 and 10 clearly shows the impact of 3D effects in the bleed hole case, compared to the 2D slot. At very low pressure ratios, the bleed hole shows similar behavior to the slot in that increasing the boundary layer thickness decreases the flow coefficient. When the ratio exceeds a critical point (in the vicinity of P_b/P_t=0.02), however, this behavior reverses, and increasing the boundary layer thickness increases the flow coefficient. Supersonic boundary layer bleed is the coupling of supersonic and subsonic parts of the boundary layer. For a circular bleed hole, there are three different physical bleed mechanisms: supersonic leading edge bleed, subsonic leading edge bleed, and the subsonic part of boundary layer bleed. The supersonic leading edge bleed makes the streamlines deflect into the bleed hole by generating expansion waves, and changes the bleed mass flow rate by adjusting the intensity of expansion waves through the pressure ratio, which is the dominant part of the supersonic bleed. Because the subsonic part of the boundary layer is affected by the back pressure disturbance of the bleed chamber, not only the direction of the main flow part can be bled into the bleed hole, but also part of the lateral flow. However, the location of the sound point in the turbulent boundary layer is very close to the wall (Babinsky and Harvey, 2011), which makes the subsonic part of the boundary layer occupy a small proportion, so the bleed mass flow rate is very weak. The subsonic leading edge of the bleed hole is also affected by the back pressure disturbance in the Mach cone. This can deflect the lateral flow toward the bleed hole. Fig. 11 shows that the streamlines of the supersonic leading edge at the entrance of the bleed hole are straight, indicating that it is not affected by the back pressure disturbance, but the streamlines of the subsonic leading edge deflect towards the bleed hole. Zhao et al. (2017) observed lateral flow of the circular bleed hole using the Schlieren method and nanoparticle-based planar laser scattering method (NPLS) flow visualization techniques. Bodner et al. (1996) also observed lateral flow for a 90° bleed hole of flow coefficient Q=0.035 through oil flow visualization technology. According to the above

analysis, the lateral flow originates from the part of subsonic leading edge of the circular hole and the subsonic part of the boundary layer, and this is the physical mechanism of the lateral flow observed experimentally.

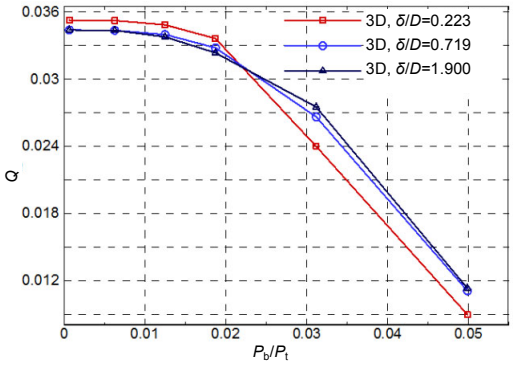

Fig. 10 Relationship between the flow coefficient and P_b/P_t with different δ/D for the bleed hole

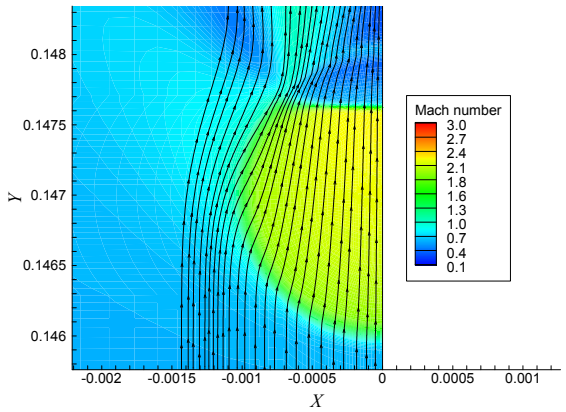

Fig. 11 Streamlines at the entrance plane of the bleed hole with D=2.0 mm and L/D=4.0

4 Evolution of flow coefficients with the bleed hole depth-to-diameter ratio L/D

Supersonic bleed can be divided into two stages: bleed choking and non-choking. They have different flow structures. The boundary layer thickness δ=2.230 mm and the bleed hole diameter D=0.6 mm, 2.0 mm, and 10.0 mm, respectively are selected to study the evolution trend of bleed flow coefficients under choking and non-choking conditions. The ratio of bleed hole depth to diameter is divided into seven working conditions, L/D=0, 0.5, 1.0, 2.0, 4.0, 8.0, and 16.0.

4.1 Effect of depth-to-diameter ratio L/D on bleed mass flow rate under non-choking condition

According to the aforementioned inflow conditions, the back pressure P_b of the bleed chamber is set 506 62.5 Pa, and the ratio of the static pressure of the bleed chamber to the inflow static pressure satisfies P_b/P_1=0 .5. The evolution of flow coefficients with depth-to-diameter ratio for different bleed hole diameters under non-choking conditions is shown in Fig. 12. The evolution trends of the flow coefficients of the three bleed holes under three different diameters are similar, i.e. decrease first, then increase, and then gradually decrease slowly, which indicates that the flow field structure of the three bleed holes is similar.

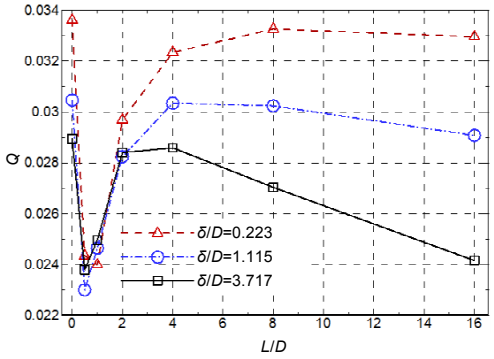

Fig. 12 Relationship between the flow coefficient and L/D for different bleed hole diameters under non-choking condition

The case of L/D=0 serves as a baseline, which corresponds to an infinitely thin bleed hole. When the streamline enters the bleed hole, it does not deflect and there is no barrier shock in the bleed hole. When the bleed hole has a finite depth, a barrier shock is formed at the entrance of the bleed hole as shown in Fig. 13. This reduces the bleed mass flow rate.

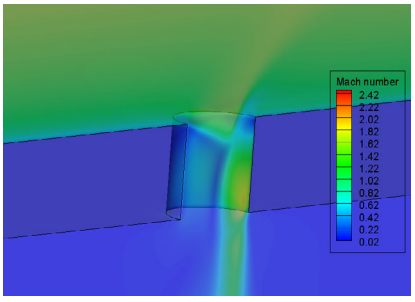

Fig. 13 Mach number contours of D=0.6 mm, L/D=2 case

For the same L/D, the smaller the boundary layer thickness to diameter ratio, the larger the bleed flow coefficient, with the exception of L/D=0.5 and 1.0. This is because a certain boundary layer thickness δ corresponds to a certain displacement thickness δ^* as shown in Fig. 14, which makes the supersonic boundary layer flow equivalent to a uniform flow at a distance of displacement thickness δ^* from the wall. So the influence of the boundary layer on the bleed mass flow rate can be transformed into the influence of the displacement thickness on the effective size of the bleed hole, reducing the bleed hole diameter. The smaller the bleed hole diameter is, the more obvious the viscous effect, and the more obviously the bleed flow coefficient decreases.

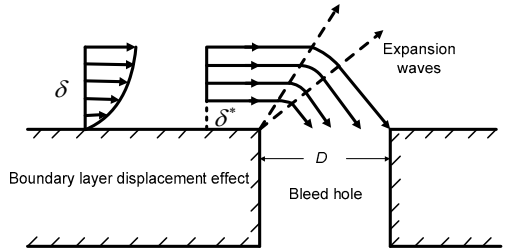

Fig. 14 Displacement thickness reduces the effective bleed hole diameter

When L/D is greater than 0.5 and less than 4.0, the bleed flow coefficient increases with the increase of depth-to-diameter ratios. Fig. 15 is a Mach number contour of the bleed hole symmetrical plane with D=2.0 mm and L/D=1.0. This shows that the air in the bleed chamber back flows to the bleed hole, while Fig. 16 is the Mach number contour of the symmetrical plane of the same diameter bleed hole with L/D=4.0, indicating that there is no back flow phenomenon. Back flow results in reduced bleed mass flow rate at L/D=1.0 but not at L/D=4.0, because when the ratio of depth to diameter is less than a certain degree, the separation zone in the bleed hole is in an open state, so the bleed chamber gas can back flow into the bleed hole. Zhao et al. (2017) also experimentally showed that the separation zone has opening and closing states under different depth-to-diameter ratios. When L/D is greater than 4.0, the flow coefficient decreases with the increase of depth-to-diameter ratio, and the larger the boundary layer thickness-to-diameter ratio, the more obviously the bleed flow coefficient decreases. This is because with the development of the boundary layer, the effective stream tube captured by the bleed hole decreases, resulting in the decrease of bleed mass flow rate. The smaller the bleed hole diameter is, the more obvious the viscous effect is.

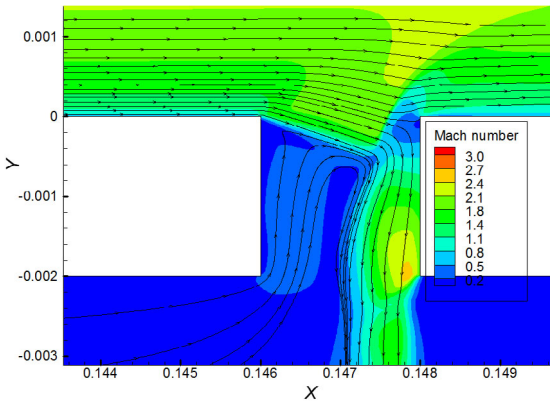

Fig. 15 Mach contours of the bleed hole symmetry plane with diameter D=2.0 mm and L/D=1.0

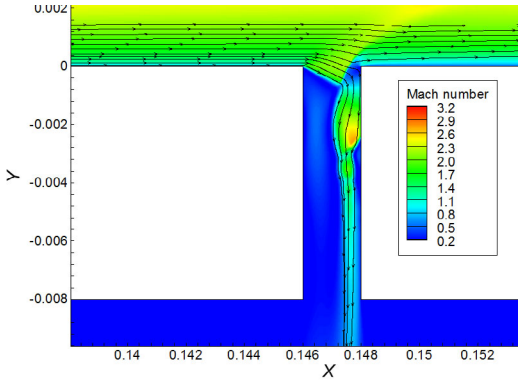

Fig. 16 Mach contours of the bleed hole symmetry plane with diameter D=2.0 mm and L/D=4.0

For the three bleed holes, when the ratios of depth to diameter are L/D=0.5 and 1.0, the flow coefficients have only a difference of about 1%, but the area of the bleed hole with D=10 mm is approximately 278 times that of the bleed hole with D=0.6 mm, which indicates that the bleed flow coefficient has a independent effect under some ratios of depth to diameter. Davis et al. (1997) also showed that when L/D=1.0, the variation of flow coefficients was very weak for the three scale bleed holes with diameters of D=6.350, 0.368, and 0.239 mm.

4.2 Effect of depth-to-diameter ratio *L*/*D* on bleed mass flow rate under choking condition

When the incoming flow static pressure, temperature, and Mach number are given, the bleed mass flow rate increases gradually with the decrease of back pressure of bleed chamber, but when the back pressure decreases to a certain extent, the bleed mass flow rate no longer increases with the decrease of back pressure. This is called supersonic bleed choking (Tan et al., 2009). The air of the hypersonic inlet is compressed by multiple shock waves generated by the forebody, so the pressure is very high, while the back pressure of the bleed system is the atmospheric pressure under the flight conditions of the aircraft, which is very low. So supersonic bleed choking is a typical working state of the hypersonic inlet bleed system.

According to the Prandtl-Meyer (P-M) expansion wave theory (Anderson, 2003), the conditions of bleed choking can be deduced when the viscous effect is ignored. For a given inflow Mach number Ma_1 and static pressure P_1, Ma_2 and P_2 are the Mach number and static pressure after the last expansion wave. The angle between the two expansion waves is φ, as shown in Fig. 17.

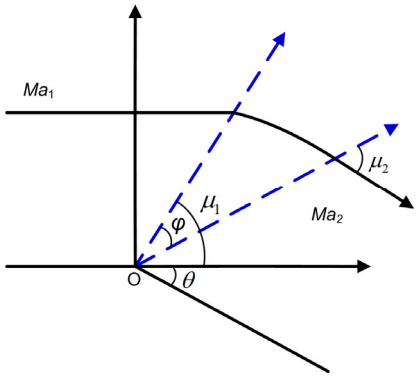

Fig. 17 Supersonic bleed chocking model

The two Mach angles μ_1 and μ_2 corresponds to the first expansion wave and the last expansion wave, respectively, which can be obtained as

$$\mu_1 = \arcsin\left(\frac{1}{Ma_1}\right), \tag{3}$$

$$\mu_2 = \arcsin\left(\frac{1}{Ma_2}\right). \tag{4}$$

From the geometric relation shown in Fig. 17, the angle of the expansion fan is

$$\varphi = \mu_1 - (\mu_2 - \theta). \tag{5}$$

The deflection angle θ of the streamline is determined by the P-M function

$$\theta = \nu(Ma_2) - \nu(Ma_1). \tag{6}$$

When the angle of the expansion fan is equal to that of the incoming Mach angle $\varphi = \mu_1$, the last expansion wave is parallel to the entrance of the bleed hole. If the back pressure continuously decreases, the expansion fan angle also continuously increases in the bleed hole. However, the bleed mass flow rate is determined by the physical conditions at the entrance. Although the back pressure is continuously reduced, the disturbance cannot propagate upstream in supersonic flow. Therefore, the physical quantities at the entrance of the bleed hole are constant, and the bleed mass flow rate does not change with the decrease of the back pressure. This is the physical mechanism that causes bleed choking to occur. According to Eqs. (3)–(6), the Mach number satisfies the relationship when bleed choking occurs.

$$\arcsin\left(\frac{1}{Ma_2}\right) = \nu(Ma_2) - \nu(Ma_1). \tag{7}$$

The critical pressure ratio of bleed choking is determined by isentropic relation, i.e.

$$\frac{P_2}{P_1} = \left(\frac{1+\frac{\gamma-1}{2}Ma_1^2}{1+\frac{\gamma-1}{2}Ma_2^2}\right)^{\frac{\gamma}{\gamma-1}}. \tag{8}$$

According to Eqs. (7) and (8), for the Mach number of 2.46, the static pressure ratio when bleed choking occurs is 0.2698. For a circular bleed hole, there is a 3D effect, but Eq. (8) is a model for determining the choking pressure ratio which ignores the 3D effect. With the ratio of static pressure of the bleed chamber to inflow static pressure P_b/P_1=0.1 and the boundary layer thickness δ=2.230 mm, CFD calculations are carried out under bleed choking conditions. The bleed flow coefficients of different

depth-to-diameter ratios are shown in Fig. 18, which shows that there is a great difference compared with non-choking conditions as shown in Fig. 12. When bleed choking, the flow coefficient of different ratios of boundary layer thickness to bleed hole diameters decreases with the increase of the depth-to-diameter ratio. This is because the flow field structure at the entrance of bleed holes does not change. The increase of the bleed depth only affects the development of the boundary layer in the bleed hole as shown in Figs. 19 and 20. The larger the boundary layer thickness to bleed hole diameter ratio, the more obvious the flow coefficient evolution decrease trend is. When the ratio of depth to diameter is less than 2.0, the bleed flow coefficients of δ/D=1.115 and 3.717 have little difference, similar to the non-choking conditions, which also shows depth-to-diameter ratio independence. With higher δ/D values of δ/D=1.115 and 3.717, the impact of viscous effects starts to make these choking conditions act a bit more like what was seen in non-choking conditions, at least for L/D>4. The thin boundary layer case of δ/D=0.223, on the other hand, clearly shows choked behavior.

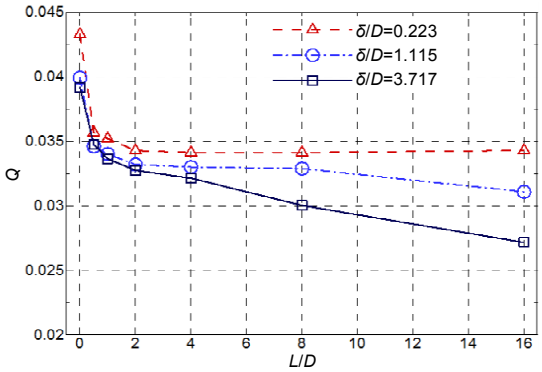

Fig. 18 Relationship between the flow coefficients and the ratio of L/D for different bleed hole diameters under choking conditions

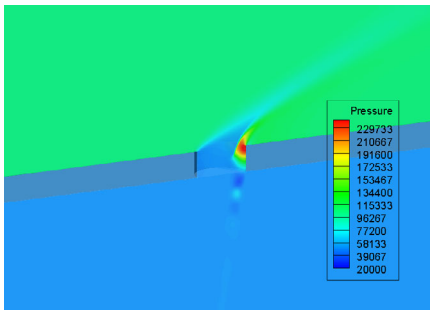

Fig. 19 Pressure contours of the bleed hole with D=2 mm and L/D=0.5 (unit: Pa)

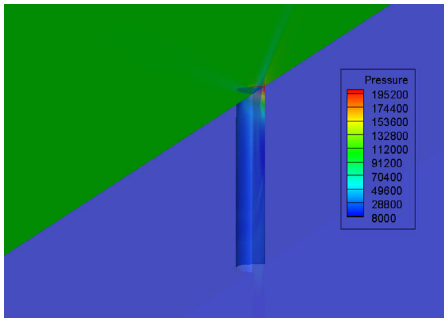

Fig. 20 Pressure contours of the bleed hole with D=2 mm and L/D=4.0 (unit: Pa)

5 Conclusions

The single bleed hole problem is extracted from the porous bleed system. The bleed hole flow structure is obtained according to the characteristics of leading edge curvature of the bleed hole. The three scales, including those of boundary layer thickness, and the depth and diameter of the bleed hole are investigated, respectively to reveal the physical mechanism that affects the bleed mass flow rate. The main conclusions are as follows:

1. Circular hole bleed includes the coupling of supersonic leading edge, subsonic leading edge, and subsonic part of supersonic boundary layer. The supersonic leading edge bleed is dominant, and the subsonic leading edge and subsonic part of supersonic boundary layer are the main reasons for lateral flow.

2. In the cases of non-choking and of choking, the flow coefficient has different evolution and development trends with the increase of depth-to-diameter ratio. Depth is the dominant factor affecting the bleed flow coefficient, and bleed hole diameter is the secondary factor.

3. In the case of non-choking, the bleed hole with a certain depth-to-diameter ratio produces back flow, which makes the flow coefficient decrease, while in the case of choking, there is no back flow phenomenon.

This paper obtains a clear physical picture of the effect of bleed scale parameters on flow coefficient, and will provide theoretical support for the design of a porous array bleed system.

Contributors

Bao-hu ZHANG wrote the first draft of this manuscript. Bao-hu ZHANG and Yu-xin ZHAO finished the numerical

simulations. Yu-xin ZHAO and Ju LIU helped to organize the manuscript.

Conflict of interest

Bao-hu ZHANG, Yu-xin ZHAO, and Jun LIU declare that they have no conflict of interest.

References

Anderson JD, 2003. Modern Compressible Flow: with Historical Perspective, 3rd Edition. McGraw Hill Education, New York, USA, p.127-187.

Babinsky H, Harvey JK, 2011. Shock Wave-Boundary-Layer Interactions. Cambridge University Press, Cambridge, UK, p.5-86.

Bodner JP, Greber I, Davis DO, et al., 1996. Experimental investigation of the effect of a single bleed hole on a supersonic turbulent boundary-layer. Proceedings of the 32nd Joint Propulsion Conference and Exhibit. https://doi.org/10.2514/6.1996-2797

Bunnag S, 2010. Bleed Rate Model Based on Prandtl-Meyer Expansion for a Bleed Hole Normal to a Supersonic Freestream. MS Thesis, University of Cincinnati, Cincinnati, USA.

Chang JT, Li N, Xu KJ, et al., 2017. Recent research progress on unstart mechanism, detection and control of hypersonic inlet. *Progress in Aerospace Sciences*, 89:1-20. https://doi.org/10.1016/j.paerosci.2016.12.001

Davis DO, Willis BE, Schoenenberger M, 1997. Porous and microporous honeycomb composites as potential boundary-layer bleed materials. Proceedings of the 33rd Joint Propulsion Conference and Exhibit. https://doi.org/10.2514/6.1997-3260

Davis DO, Vyas M, Slater J, 2012. Research on supersonic inlet bleed. Proceedings of the 50th AIAA Aerospace Sciences Meeting Including the New Horizons Forum and Aerospace Exposition. https://doi.org/10.2514/6.2012-272

Eichorn MB, Barnhart PJ, Davis DO, et al., 2013. Effect of boundary-layer bleed hole inclination angle and scaling on flow coefficient behavior. Proceedings of the 51st AIAA Aerospace Sciences Meeting Including the New Horizons Forum and Aerospace Exposition. https://doi.org/10.2514/6.2013-424

Gupta R, Hussain SA, Condoor S, et al., 2016. Numerical study on performance of scramjet intake with boundary layer bleed. *International Journal of Control Theory and Applications*, 9(17):8785-8793.

Hamed A, Manavasi S, Shin D, et al., 2011. Bleed interactions in supersonic flow. *International Journal of Flow Control*, 3(1):37-48. https://doi.org/10.1260/1756-8250.3.1.37

Hu JX, Zhang WH, Xia ZX, et al., 2013. Scramjet Propulsion Technology. Publication of National University of Defense Technology, Changsha, China, p.120-123 (in Chinese).

Im SK, Do H, 2018. Unstart phenomena induced by flow choking in scramjet inlet-isolators. *Progress in Aerospace Sciences*, 97:1-21. https://doi.org/10.1016/j.paerosci.2017.12.001

Jiao XL, 2017. Research on Hypersonic Inlet Unstart Multimodes and Mode Transition. PhD Thesis, Harbin Institute of Technology, Harbin, China (in Chinese).

Mahoney JJ, 1990. Inlets for Supersonic Missiles. American Institute of Aeronautics and Astronautics, Washington DC, USA, p.67-84.

Martin PG, Hodges J, Duveau P, et al., 2007. A Study of the Aerodynamics of a Supersonic Intake Compression Surface with Perforated Bleed Using CFD Methods. Technical Report No. GARTEUR TP 161, Group for Aeronautical Research and Technology in Europe, Europe.

Sepahi-Younsi J, Feshalami BF, Maadi SR, et al., 2019. Boundary layer suction for high-speed air intakes: a review. *Proceedings of the Institution of Mechanical Engineers, Part G: Journal of Aerospace Engineering*, 233(9):3459-3481. https://doi.org/10.1177/0954410018793262

Soltani MR, Younsi JS, Farahani M, 2015. Effects of boundary-layer bleed parameters on supersonic intake performance. *Journal of Propulsion and Power*, 31(3): 826-836. https://doi.org/10.2514/1.B35461

Syberg J, Hickcox TE, 1973. Design of a Bleed System for a Mach 3.5 Inlet. Technical Report No. NASA CR 2187, National Aeronautics and Space Administration, Washington DC, USA.

Tan HJ, Sun S, Yin ZL, 2009. Oscillatory flows of rectangular hypersonic inlet unstart caused by downstream mass-flow choking. *Journal of Propulsion and Power*, 25(1): 138-147. https://doi.org/10.2514/1.37914

Wang QC, Wang ZG, Zhao YX, 2017. The impact of streamwise convex curvature on the supersonic turbulent boundary layer. *Physics of Fluids*, 29(11):116106. https://doi.org/10.1063/1.4994928

Wang Y, 2017. Influence of Suction on Restart Characteristics of Hypersonic Inlet. MS Thesis, Harbin Institute of Technology, Harbin, China (in Chinese).

Wang ZG, Zhao YL, Zhao YX, et al., 2015. Prediction of massive separation of unstarted inlet via free-interaction theory. *AIAA Journal*, 53(4):1108-1112. https://doi.org/10.2514/1.J053501

Willis BP, Davis DO, Hingst WR, 1995. Flow coefficient behavior for boundary layer bleed holes and slots. Proceedings of the 33rd Aerospace Sciences Meeting and Exhibit. https://doi.org/10.2514/6.1995-31

Wukie NA, Orkwis PD, Turner MG, et al., 2015. Simulations and models for aspirations in a supersonic flow using overflow. *AIAA Journal*, 53(7):2052-2056. https://doi.org/10.2514/1.J053214

Zhang MZ, 2018. Bleed System Design of a Supersonic Rectangular-duct Wind Tunnel. MS Thesis, University of Florida, Gainesville, USA.

Zhang WH, Liu J, Ding F, et al., 2019. Novel integration methodology for an inward turning waverider forebody/inlet. *Journal of Zhejiang University-SCIENCE A (Applied Physics & Engineering)*, 20(12):918-926. https://doi.org/10.1631/jzus.A1900334

Zhao J, 2016. Research on Flow field Structure in Supersonic Boundary Layer Bleed Holes and Slots. MS Thesis, National University of Defense and Technology, Changsha, China (in Chinese).

Zhao J, Fan XQ, Wang Y, et al., 2017. Classification of flow field in supersonic boundary layer bleed slot. *Journal of Propulsion Technology*, 38(11):2463-2470 (in Chinese). https://doi.org/10.13675/j.cnki.tjjs.2017.11.008

Zhao YL, 2014. Study of Separated Flow Modeling and Unstart Mechanism of Hypersonic Inlet. PhD Thesis, National University of Defense Technology, Changsha, China (in Chinese).

中文概要

题　目： 抽吸孔尺度对超声速边界层抽吸流量的影响

目　的： 在超声速来流条件下，探索影响抽吸流量的关键参数，为高超声速进气道抽吸系统的设计提供参考。

方　法： 1. 从抽吸系统提取出边界层厚度、抽吸孔径和深度三个尺度，并采用单变量原则，通过数值模拟分别研究三个尺度对抽吸流量的影响；2. 采用普朗特-迈耶膨胀波理论，根据抽吸流动是由压差驱动的物理机制，建立超声速抽吸壅塞模型。

结　论： 1. 超声速圆孔抽吸包括超声速前缘、亚声速前缘和边界层中的亚声速部分三种抽吸物理机制；2. 在非壅塞与壅塞条件下，随着孔径与深度比值的变化，流量系数具有不同的演化规律；3. 深度是影响抽吸流量的主要因素，孔径是次要因素；4. 在一定的孔径深度比值下，抽吸在非壅塞条件下具有回流现象，而在壅塞条件下不具有回流现象。

关键词： 超声速抽吸；壅塞；尺度效应；抽吸质量流率；进气道；横向流动